VESSEL PREP, STEP BY STEP.

DESIGNED TO TREAT 360° OF THE VESSEL.

WATCH IT NOW

Important Safety Information

CSI® | CARDIOVASCULAR SYSTEMS, INC.

Catheterization and Cardiovascular Interventions 89:932–943 (2017)

VALVULAR AND STRUCTURAL HEART DISEASES

Original Studies

Relationship of Mitral Valve Annulus Plane and Circumflex-Right Coronary Artery Plane: Implications for Transcatheter Mitral Valve Implantation

Samir R. Kapadia,[1*] MD, Amgad Mentias,[1] MD, Amr F. Barakat,[1] MD, Mohammad Q. Raza,[1] MD, Kanhaiya Lal Poddar,[1] MD, Cristian Baeza,[2] MD, Gabriel Maluenda,[2] MD, Jose Navia,[1] MD, Paul Schoenhagen,[1] MD, and E. Murat Tuzcu,[1] MD

Aim: Transcatheter mitral valve implantation (TMVI) is a novel technology for patients with severe mitral valve disease but at high surgical risk. Imaging guidance during the procedure is critical for successful device deployment. Identification of the mitral annular plane (MAP) with fluoroscopy during the procedure is limited by lack of clearly defined landmarks. We hypothesized that a plane defined by left circumflex-right coronary arteries (LCX-RCA) would have a consistent relationship to MAP. Methods and results: We studied 25 patients with gated cardiac computed tomography. We identified the MAP and the LCX-RCA plane in mid systole and diastole. The distance between the two planes in prespecified four points (anterior, posterior, medial, and lateral) in the apical 2 and 3-chamber views. Alignment of the planes was described by cranial/caudal angulation for both planes in RAO 30° and LAO 90° (lateral) angulation. Mean age was 81 ± 9 years, 56% of patients had ≥2+ mitral regurgitation. In mid systole, the distances between the LCX-RCA plane and the MAP in the four points were < 5 mm in 92% of patients. In mid diastole, distances were < 5 mm in 100% of patients. In mid systole, the correlation between the caudal/cranial orientations of the 2 planes was 0.85 and 0.80 in the LAO 90° and RAO 30°, respectively ($P = <0.001$). In mid diastole, this was 0.92 and 0.92 in the LAO 90° and RAO 30°, respectively ($P = <0.001$). Conclusion: LCX-RCA plane has a close and consistent relationship to the MAP and can be useful to guide TMVI. Accurate imaging of mitral valve annular plane during TMVI procedure is challenging. MAP guided by fluoroscopy might be crucial to guide successful prosthesis deployment. A plane defined by the left circumflex- right coronary arteries in the atrioventricular grove has a consistent relationship with MAP; this can be used aided by pre-procedural MDCT to guide TMVI procedure.

Key words: mitral valve; transcatheter mitral valve implantation; mitral valve imaging; cardiac computed tomography

---

[1]Department of Cardiovascular Medicine, Heart and Vascular Institute, Cleveland Clinic Foundation, Ohio
[2]Department of cardiovascular medicine, San Borja Arriaran Hospital, Cardiovascular Center, Santiago, Chile

Conflict of Interest: Nothing to report.

*Correspondence to: Samir R. Kapadia, MD, Professor of Medicine Director, Sones Cardiac Catheterization Laboratories, Department of Cardiovascular Medicine, J2-3 Heart and Vascular Institute Cleveland Clinic, 9500 Euclid Avenue, Cleveland, OH 44195. E-mail: kapadis@ccf.org

Received 5 October 2015; Revision accepted 22 April 2016

DOI: 10.1002/ccd.26575
Published online 24 May 2016 in Wiley Online Library (wileyonlinelibrary.com)

INTRODUCTION

Transcatheter Mitral Valve Implantation (TMVI) is a novel evolving technology for patients with severe mitral valve disease that are at high-risk for surgical intervention. Recently, first in man experiences of TMVI have been reported after extensive animal experiments [1–14]. The development of this percutaneous technique has been influenced by the experience with Transcatheter Aortic Valve Replacement (TAVR) [15–17].

The TAVR experience has demonstrated that transcatheter device deployment is largely dependent on pre-procedural and intraprocedural imaging. Accurate valve deployment requires coaxial alignment of the fluoroscopic imaging plane to aortic annular plane. The aortic annular plane can be determined using pre-procedural multidetector computed tomography (MDCT). This plane is then confirmed with aortography and fluoroscopy during the procedure [18]. The annular plane of a tricuspid aortic valve is easily visualized on fluoroscopy based on clear well defined anatomic landmarks [19]. Similar fluoroscopic guidance for TMVI procedure is more challenging, even after determining mitral annular plane (MAP) on MDCT. The main reason is the lack of anatomic landmarks for fluoroscopic confirmation. Opacification of the left atrium or ventricle requires substantial contrast load. Placing a wire in the coronary sinus is limited due to anatomical variation and proximity of the coronary sinus only to the lateral aspect of the fluoroscopic annular plane [20–23].

In TMVI procedures currently reported, prosthesis positioning has been guided mainly with 3-D transesophageal echocardiography (TEE). Although, TEE has its own inherited limitations, it remains critical for intra-procedural guidance. Nonetheless, mitral valve prosthesis positioning might be more reliable if two modalities exist to complement each other. Fluoroscopy would have a lot more to add given the complexity of mitral valve anatomy.

We hypothesized that a plane defined by left circumflex-right coronary artery (LCX-RCA) could provide a consistent relationship to MAP to guide TMVI. In this study, we sought the relationship of LCX-RCA plane to MAP in systole and diastole based on MDCT.

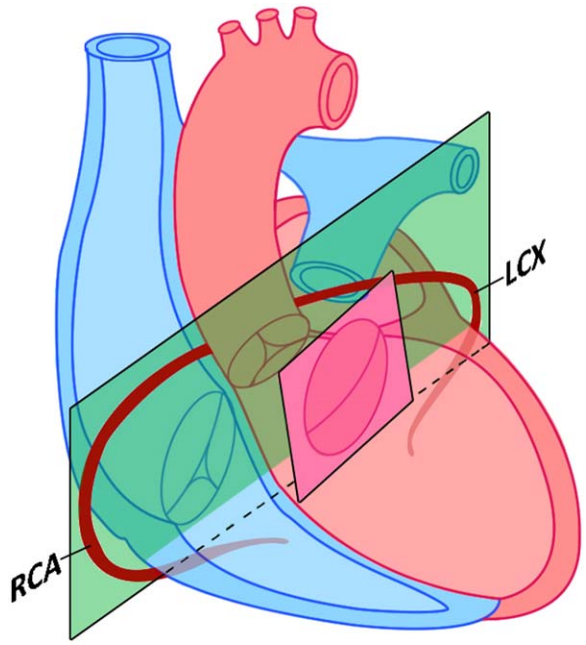

Fig. 1. Illustrative diagram showing the relation between the mitral annulus plane and the LCX-RCA plane. [Color figure can be viewed in the online issue, which is available at wileyonlinelibrary.com.]

METHODS

We retrospectively identified 25 patients who had contrast-enhanced gated cardiac MDCT in our institution. All procedures and data collection were approved and monitored by the Cleveland Clinic Institutional Review Board with waiver of individual informed consent.

Image Acquisition

All subjects were scanned on clinical MDCT scanners (Definition Dual Source/Definition Flash, Siemens Medical Solutions, Erlangen, Germany; or Brilliance 256-slice, Philips Medical Systems, Best, The Netherlands). For the contrast enhancement, 50 mL of iodinated contrast (Ultravist 370) was administered at 4–5 mL/sec through the antecubital vein followed by 30–50 mL of normal saline. Scan range extended from the carina to the diaphragm during a single inspiratory breath hold. Spiral data was acquired with retrospective electrocardiogram gating using the following parameters: gantry rotation time = 270 to 330 msec; beam collimation ranging from 128 × 0.6 mm to 32 × 0.6 mm; tube voltage = 100 to 120 kVp; tube current adjusted per patient weight; and beam pitch of 0.2 to 0.5. Electrocardiogram-based tube current modulation was used for all patients, with maximum current turned on between 30 and 70% phases of the cardiac cycle. Images were reconstructed in 10% intervals through the cardiac cycle with a section thickness of 0.75 mm.

Measurements

Figure 1 is a diagrammatic illustration of the spatial relation between the two planes of interest; MAP (shown in pink) and LCX-RCA plane (shown in green).

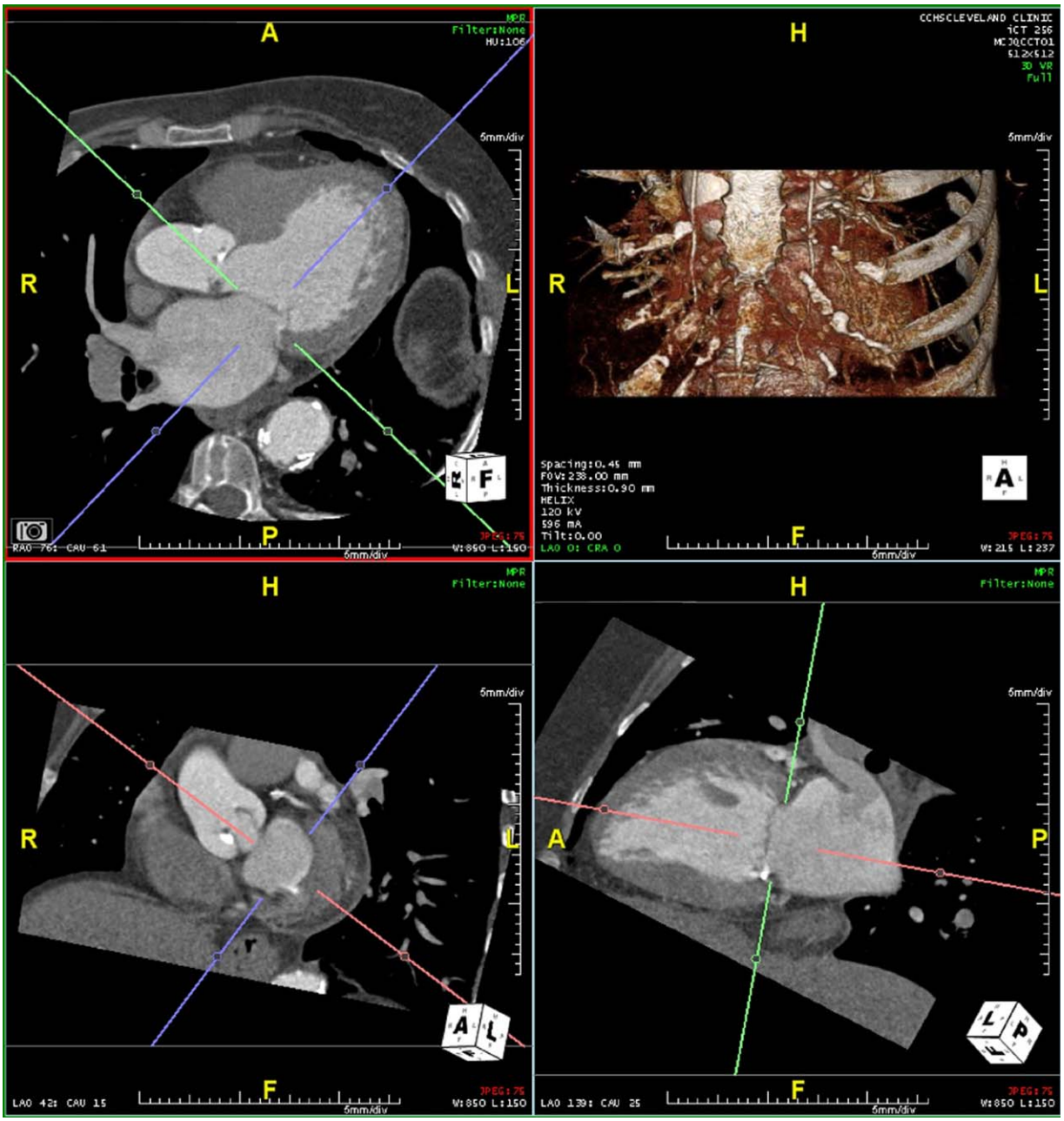

Fig. 2. Axial plane (green line) is adjusted exactly on the mitral annulus plane in the apical three-chamber view (upper left) and in the apical two-chamber view (lower right). The axial plane panel is now showing the mitral valve annulus plane (lower left). [Color figure can be viewed in the online issue, which is available at wileyonlinelibrary.com.]

Measurements were performed using Aquarius iNtuition 4.4 software (TeraRecon, San Mateo, CA). Step 1: Reconstructed images were manually reoriented into standard 2-dimensional planes; 2-chamber (2C) and 3-chamber (3C) views (Fig. 2). Step 2: the axial plane was adjusted on the MAP in 2C and 3C views; relying on the points of mitral leaflets insertion (Fig. 2). Step 3: Once the MAP was defined in the axial plane panel (Fig. 2, lower left), the long axis planes were rotated in that panel to record the specific cranial and caudal angulations for the MAP in Left Anterior Oblique (LAO) 90° and Right Anterior Oblique (RAO) 30° projections.

Coronary arteries were manually tracked and reconstructed using 3-dimensional mapping and the courses

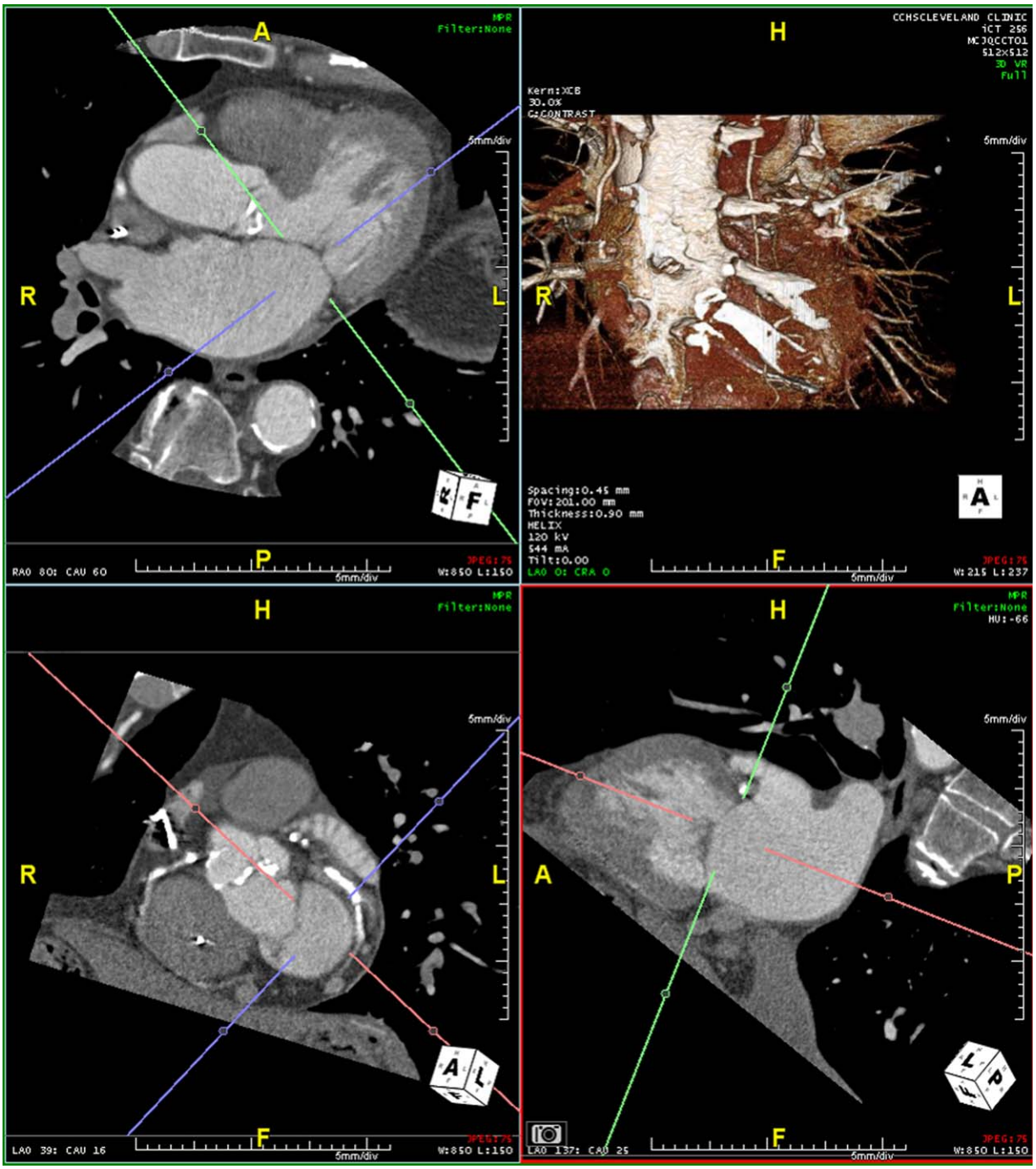

Fig. 3. Axial plane is adjusted to show the left circumflex artery and the right coronary artery simultaneously in the atrio-ventricular groove (lower left). This axial double oblique plane level and orientation (green line) is shown in the apical three-chamber view (upper left) and the apical two-chamber view (lower right). [Color figure can be viewed in the online issue, which is available at wileyonlinelibrary.com.]

of RCA and LCX in the atrio-ventricular groove were examined to guide further steps. Step 4: Another double oblique axial plane was reconstructed cutting through the portions of LCX and RCA in the atrio-ventricular groove (LCX-RCA plane; Fig. 3, lower left). Step 5: In the axial plane panel, the long axis planes were rotated to record the specific cranial and caudal angulations for the LCX-RCA plane in LAO 90° and RAO 30° projections; similar to what was done in step 3.

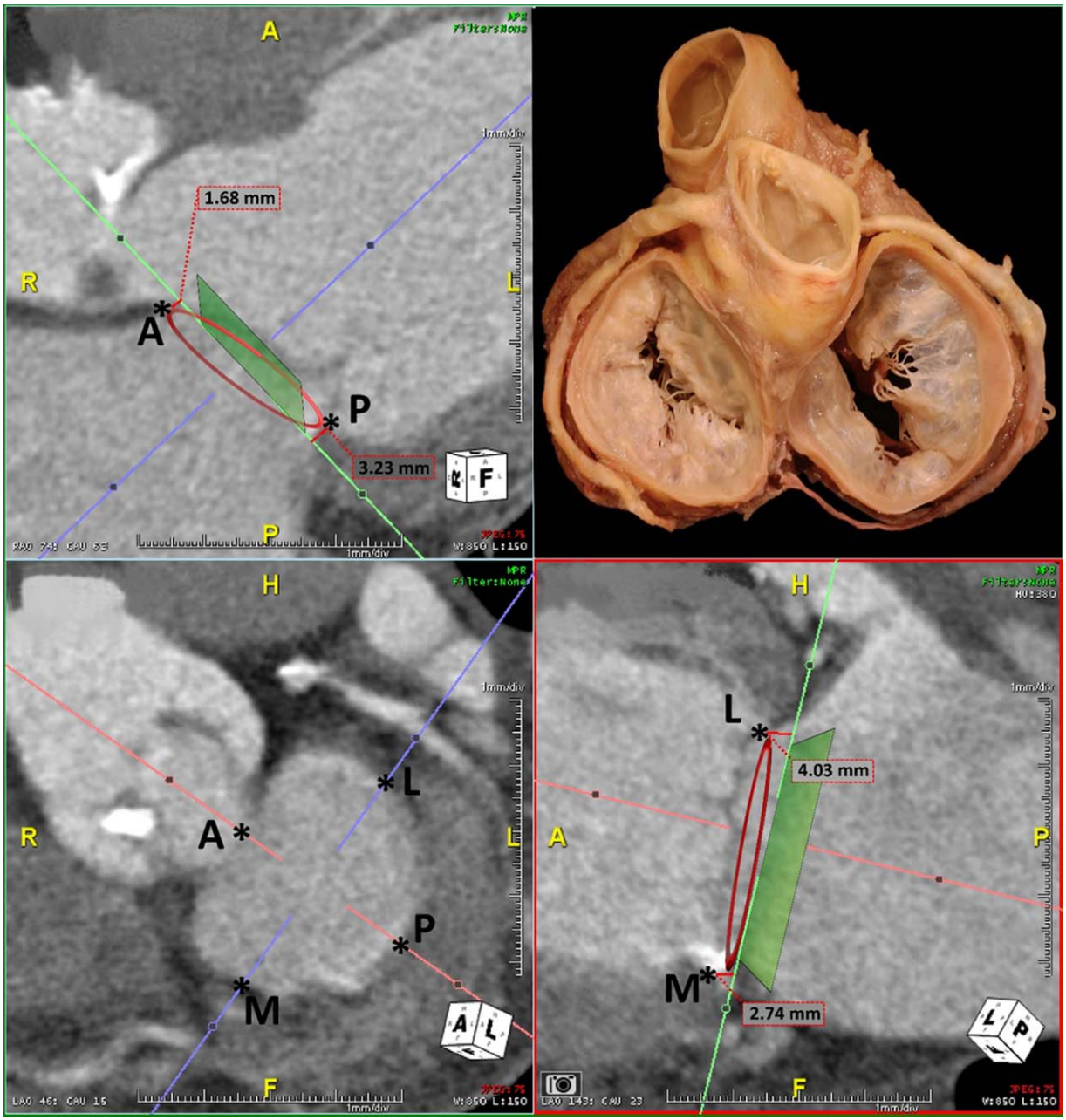

Fig. 4. The LCX-RCA double oblique axial plane (lower left). Distance from this plane (green line) to the mitral valve annulus (*) in the previously described four points; anterior "A" and posterior "P" (apical three-chamber view, upper left) and medial "M" and lateral "L" (in apical two-chamber view, lower right). Autopsy showing the LCX-RCA plane (upper right). [Color figure can be viewed in the online issue, which is available at wileyonlinelibrary.com.]

Step 6: While keeping the LCX-RCA plane in the previously described axial plane panel, the long-axis planes were again rotated into standard 2C and 3C views (Fig. 3). Step 7: in 2C and 3C views, the distance in millimeters was measured between the LCX-RCA plane (green line in Figs. 3 and 4) and the mitral annulus (defined by the points of mitral leaflets insertion) at 4 points: anterior (A), posterior (P), medial (M), and lateral (L) as shown in Fig. 4.

The previously described steps and measurements were performed both in mid-systole (30% R-R interval) and mid-diastole (70% R-R interval) phases of the ECG-gated CT scans.

TABLE I. Study Population Characteristics

Age	81.324 ± 8.79 year
Gender	44% males
Hypertension	96%, (*N* = 24)
Diabetes	36%, (*N* = 9)
Hyperlipidemia	76%, (*N* = 19)
CAD	96%, (*N* = 24)
CABG	28%, (*N* = 7)
EF	53.4 ± 10.2%
LVEDV	96 ± 34.6 ml
LVESV	41.4 ± 20.2 ml
LVIDd	45.3 ± 8.9 mm
LVIDs	31.4 ± 9.4 mm
LAV	83.5 ± 31.4 ml
LAVI	46.2 ± 17.4 ml/m^2
BMI	26.788 ± 7.38 kg/m^2

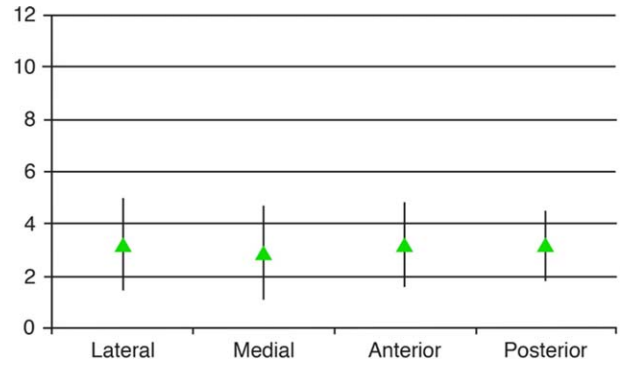

Fig. 5. Distances from the LCX-RCA plane to the mitral valve annulus in systole anteriorly, posteriorly, medially, and laterally were 3.2 ± 1.6, 3.2 ± 1.3, 2.9 ± 1.8, and 3.2 ± 1.7 mm, respectively. [Color figure can be viewed in the online issue, which is available at wileyonlinelibrary.com.]

TABLE II. Comparison between Patients with <2 MR and Those with ≥2 MR Regarding Distances between the Two Planes in the Four Prespecified Points

	Mid systole			Mid diastole		
	≥2 MR	<2 MR	*P* Value	≥2 MR	<2 MR	*P* Value
Anterior	3.1 ± 1.1	3.4 ± 2.1	0.6	2.5 ± 1.1	2.4 ± 1	0.8
Posterior	2.8 ± 1.2	3.9 ± 1.2	0.03	2.6 ± 1.3	3.4 ± 0.7	0.08
Medial	2.3 ± 1.2	3.9 ± 2	0.04	2.5 ± 1	2.8 ± 1.1	0.6
Lateral	2.9 ± 1.7	3.8 ± 2.2	0.2	2.5 ± 1.1	2.7 ± 1.1	0.7

Intraobserver and Interobserver Variability

All angle projections and distances between the LCX-RCA plane and the four points were initially performed by one blinded observer, after a 7 weeks interval, all measurements were repeated by the same observer and a second observer for 10 patients.

Statistical Analysis

Descriptive statistics are presented as mean values and SD for continuous variables and as frequencies and percentages for categoric variables. Continuous variables were compared using Spearman's correlation test. A *P* value of <0.05 was considered statistically significant. All analyses were performed using JMP statistics software package. The Bland-Altman analysis was performed to evaluate agreement between measurements and to assess intraobserver and interobserver variability [24].

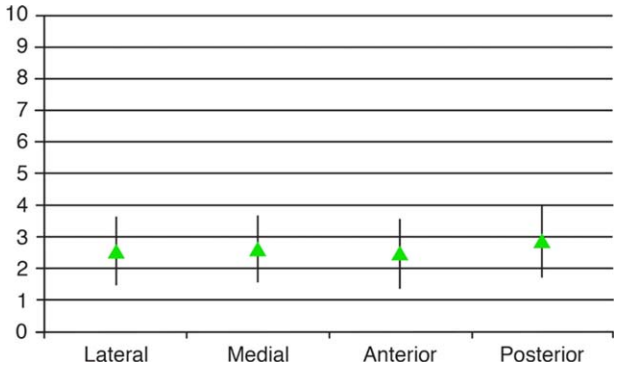

Fig. 6. Distances from the LCX-RCA plane to the mitral valve annulus in diastole anteriorly, posteriorly, medially, and laterally were 2.5 ± 1.1, 2.9 ± 1.1, 2.6 ± 1, and 2.6 ± 1.1 mm, respectively. [Color figure can be viewed in the online issue, which is available at wileyonlinelibrary.com.]

RESULTS

Patient Population

Patients' characteristics are provided in Table I, mean age was 81.3 ± 8.8; ≥2+ MR was present in 15 (60%) patients. Mean ejection fraction (EF) was 53.4 ± 10.2%, Mean Left ventricular end-systolic volume (LVESV), end-diastolic volume (LVEDV), internal diastolic diameter (LVIDd), internal systolic diameter (LVIDs), left atrial volume (LAV) and volume index (LAVI) were 41.4 ± 20.2 ml, 96 ± 34.6 ml, 45.3 ± 8.9 mm, 31.4 ± 9.4 mm, 83.5 ± 31.4 ml and 46.2 ± 17.4 ml/m2 respectively.

Separation between LCX-RCA Plane and the Mitral Annulus

In mid systole, the distances between the LCX-RCA plane and the mitral annulus anteriorly, posteriorly, medially and laterally were 3.2 ± 1.6, 3.2 ± 1.3, 2.9 ± 1.8, and 3.2 ± 1.7 mm, respectively (Fig. 5). The distances were <5 mm in 92% of the pts.

When only patients with ≥2 MR were analyzed, distances anteriorly, posteriorly, medially, and laterally were 3.1 ± 1.1, 2.8 ± 1.2, 2.3 ± 1.2, and 2.9 ± 1.4 mm, respectively (Table II).

In mid diastole, the distances between the LCX-RCA plane and the mitral annulus anteriorly, posteriorly, medially, and laterally were 2.5 ± 1.1, 2.9 ± 1.1, 2.6 ± 1, and 2.6 ± 1.1 mm, respectively (Fig. 6), these distances were <5 mm in 100% of the patients.

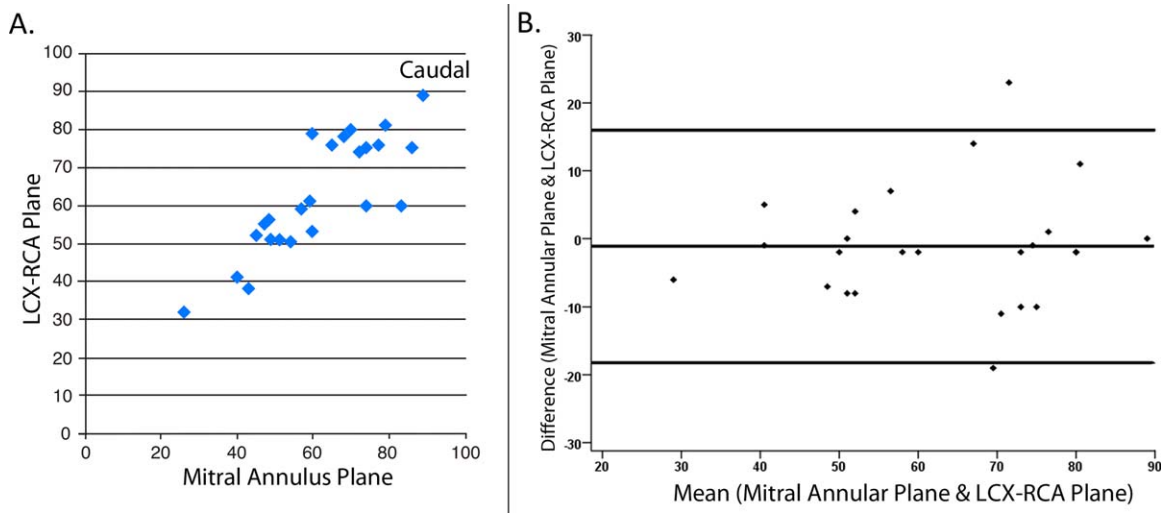

Fig. 7. A: Correlation between cranial/caudal angulation of the LCX-RCA plane and the mitral valve annulus plane in the LAO 90° projection in mid systole. $r = 0.85$, $P = <0.001$. B: The corresponding Bland-Altman plot; coefficient = 0.05, $P = 0.68$. [Color figure can be viewed in the online issue, which is available at wileyonlinelibrary.com.]

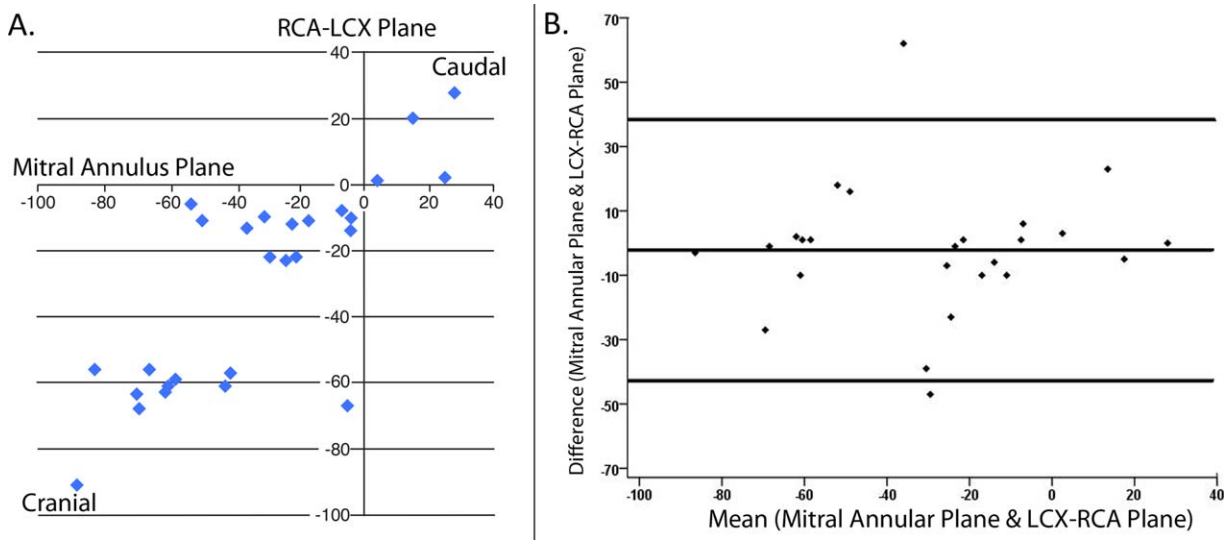

Fig. 8. A: Correlation between cranial/caudal angulation of the LCX-RCA plane and the mitral valve annulus plane in the RAO 30° projection in mid systole. $r = 0.8$, $P = <0.001$. B: The corresponding Bland-Altman plot; coefficient = 0.04, $P = 0.79$. [Color figure can be viewed in the online issue, which is available at wileyonlinelibrary.com.]

When only patients with ≥2 were analyzed, distances anteriorly, posteriorly, medially, and laterally were 2.5 ± 1.1, 2.6 ± 1.3, 2.5 ± 1, and 2.5 ± 1.1 mm, respectively (Table II).

Relation of LCX-RCA Plane to Mitral Valve Annulus Plane

In mid systole, the correlation between the caudal/cranial orientations of the 2 planes was 0.85 and 0.80 in LAO 90° and RAO 30°, respectively ($P = <0.001$ for both; Figs. 7A and 8A). Further, 80% and 68% of patients had a MVA plane within 10° (caudal/cranial) of the LCX-RCA plane in LAO 90 and RAO 30 projections, respectively; 96 and 80% of patients had it within 20° in those same projections, respectively.

When only patients with ≥2 MR were analyzed, the correlation between the caudal/cranial orientations of

TABLE III. Comparison between Patients with <2 MR and Those with ≥2 MR Regarding Correlation of Planes in Different Projections

Mid systole						Mid diastole					
LAO 90			RAO 30			LAO 90			RAO 30		
≥2 MR	<2 MR	*P* Value	≥2 MR	<2 MR	*P* Value	≥2 MR	<2 MR	*P* value	≥2 MR	<2 MR	*P* Value
0.85	0.85	0.8	0.81	0.77	0.6	0.98	0.86	0.7	0.94	0.83	0.3

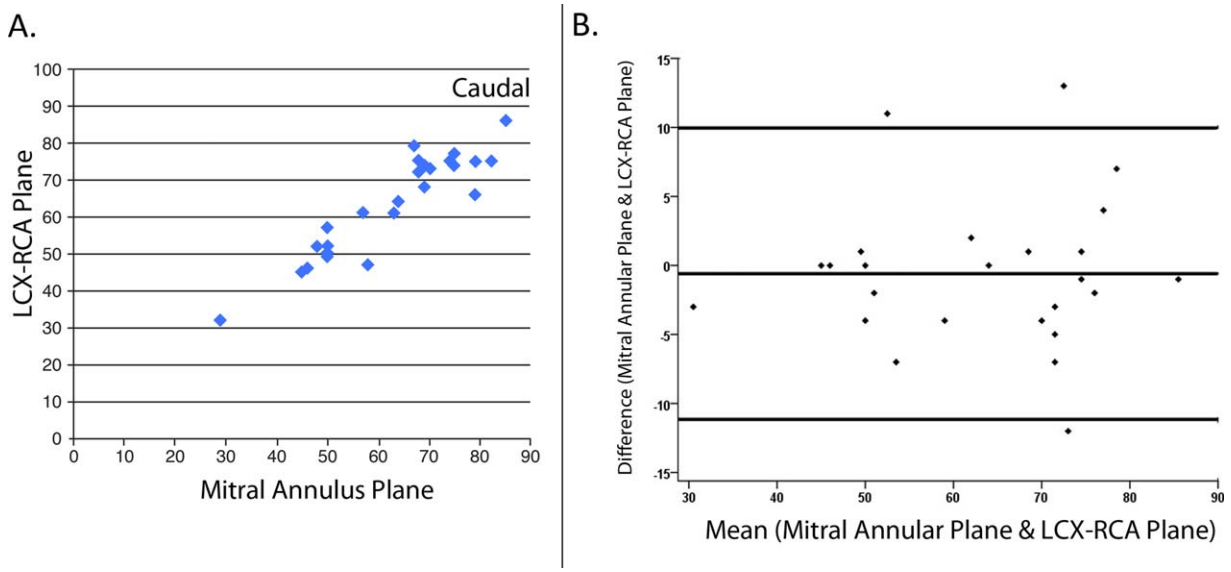

Fig. 9. A: Correlation between cranial/caudal angulation of the LCX-RCA plane and the mitral valve annulus plane in LAO 90° projection in mid diastole. $r = 0.92$, $P = <0.001$. B: The corresponding Bland-Altman plot; coefficient = 0.02, $P = 0.795$. [Color figure can be viewed in the online issue, which is available at wileyonlinelibrary.com.]

the two planes was 0.85 and 0.81 in LAO 90 and RAO 30, respectively (Table III).

In mid diastole, the correlation between the caudal/cranial orientations of the 2 planes was 0.92 and 0.92 in LAO 90° and RAO 30°, respectively ($P = <0.001$ for both; Figs. 9A and 10A); 88 and 68% of patients had a MVA plane within 10° (caudal/cranial) of the LCX-RCA plane in LAO 90 and RAO 30 projections, respectively, 100% and 92% of patients had it within 20° in those same projections, respectively.

When only patients with ≥2 MR were analyzed, the correlation between the caudal/cranial orientations of the two planes was 0.98 and 0.94 in LAO 90° and RAO 30°, respectively (Table III).

Furthermore, Bland Altman graphs were plotted to further elucidate the linear relationship and to rule out any bias (Figs. 7B, 8B, 9B, and 10B). The unstandardized coefficient ranged from 0.02 to 0.05 (close to 0.01) for all relationships. The presence of systematic error was not confirmed since zero was included in the 95% CI and the points were symmetrically distributed around the zero on the Bland-Altman plot. In addition, *P*-values obtained through linear regression of difference over means were not significant in any of the plots, thus ruling out any proportional bias.

Intraobserver and Interobserver Variability

Mean difference by Bland-Altman analysis for both repeat measurements by the same and second observer are listed in Table IV.

DISCUSSION

This study demonstrated that it is feasible to reconstruct a plane defined by left circumflex and right coronary arteries as they traverse the atrio-ventricular groove. This LCX-RCA plane appears to correlate reliably with the mitral valve annulus plane in both mid systole and mid diastole. The distance between the former plane and the mitral annulus is variable but yet

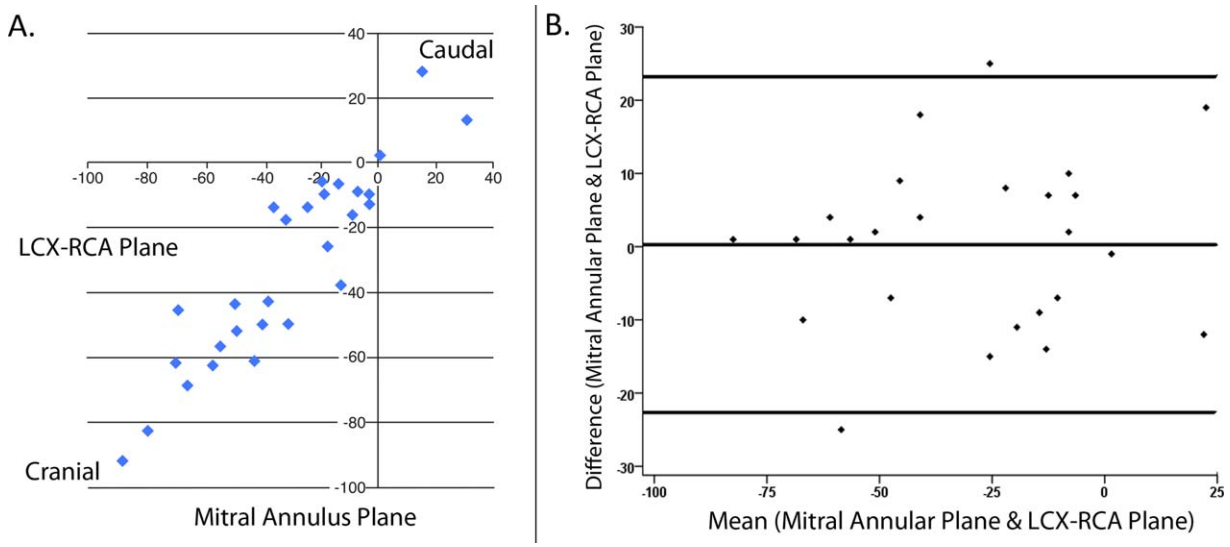

Fig. 10. A: Correlation between cranial/caudal angulation of the LCX-RCA plane and the mitral valve annulus plane in the RAO 30° projection in mid diastole. $r = 0.92$, $P = <0.001$. B: The corresponding Bland-Altman plot; coefficient = 0.05, $P = 0.58$. [Color figure can be viewed in the online issue, which is available at wileyonlinelibrary.com.]

TABLE IV. Mean Difference with Standard Deviation Regarding Interobserver and Intraobserver variability

Variable	Intraobserver agreement, mean ± SD (95% CI)	Interobserver agreement, mean ± SD (95% CI)
MA RAO 30 (°)	−3.6 ± 2 (−7.9 to 0.8)	4.0 ± 2.4 (−1.4 to 9.0)
MA LAO 90 (°)	0.4 ± 2 (−4 to 4.5)	−2.6 ± 1.5 (−5.9 to 0.74)
LCX-RCA RAO 30 (°)	−2.4 ± 2 (−7 to 2)	1.9 ± 2.1 (−2.8 to 6.5)
LCX-RCA LAO 90 (°)	−0.6 ± 1.9 (−4.7 to 3.6)	−2.1 ± 1.8 (−6.1 to 2)
Lateral Distance (mm)	−0.1 ± 0.4 (−0.9 to 0.7)	−0.1 ± 0.5 (−0.9 to 0.8)
Medial distance (mm)	0.1 ± 0.4 (−0.8 to 0.9)	−0.2 ± 0.4 (−0.9 to 0.6)
Anterior Distance (mm)	−0.4 ± 0.2 (−0.7 to 0.1)	0.2 ± 0.3 (−0.4 to 0.9)
Posterior distance (mm)	−0.1 ± 0.4 (−0.9 to 0.7)	−0.05 ± 0.3 (−0.6 to 0.5)

definable, and in all patients was found to be <5 mm as measured in 4 predefined locations.

Prior data from our group, evaluating the relationship between mitral annulus and coronary sinus demonstrated significantly large and less consistent distance between the two structures, indicating that the coronary sinus plane is not parallel to the MAP [22]. These findings were subsequently confirmed by several other studies [21,25]. The focus of these studies was to predict if devices deployed in the coronary sinuses would be able to change the geometry of the mitral annulus to decrease the degree of mitral regurgitation. In contrast, with TMVI, it is critical to define the mitral annulus based on consistent anatomical landmarks. The coronary sinus is a limited landmark due to the fact that its relationship is limited to the lateral aspect of the mitral annulus. Therefore, precise alignment of the fluoroscopic planes is challenging. Furthermore, the significant variation in distance and trajectory of coronary sinus in relation to mitral annulus as defined in prior studies makes its use even more challenging.

In the TAVR experience, procedural planning with MDCT has become an integral part of the procedure. Based on dedicated reconstruction of the 3-D dataset, CT allows to predict fluoroscopic projection angles, which are coaxial to the aortic valve [18,19]. This preprocedural data is verified by the interventionist during the procedure using aortic root angiography. In TMVI, the area that would need to be opacified with contrast, either left ventricle or left atrium, is large and the annulus lacks clear landmarks.

Optimum positioning of the valve would theoretically reduce the risk of mechanical complications including paravalvular leakage (PVL), embolization and insufficient deployment. PVL is much less tolerated in the mitral position compared to the aortic. In most of the TMVI animal and human cases reported until now, TEE was the main modality to determine

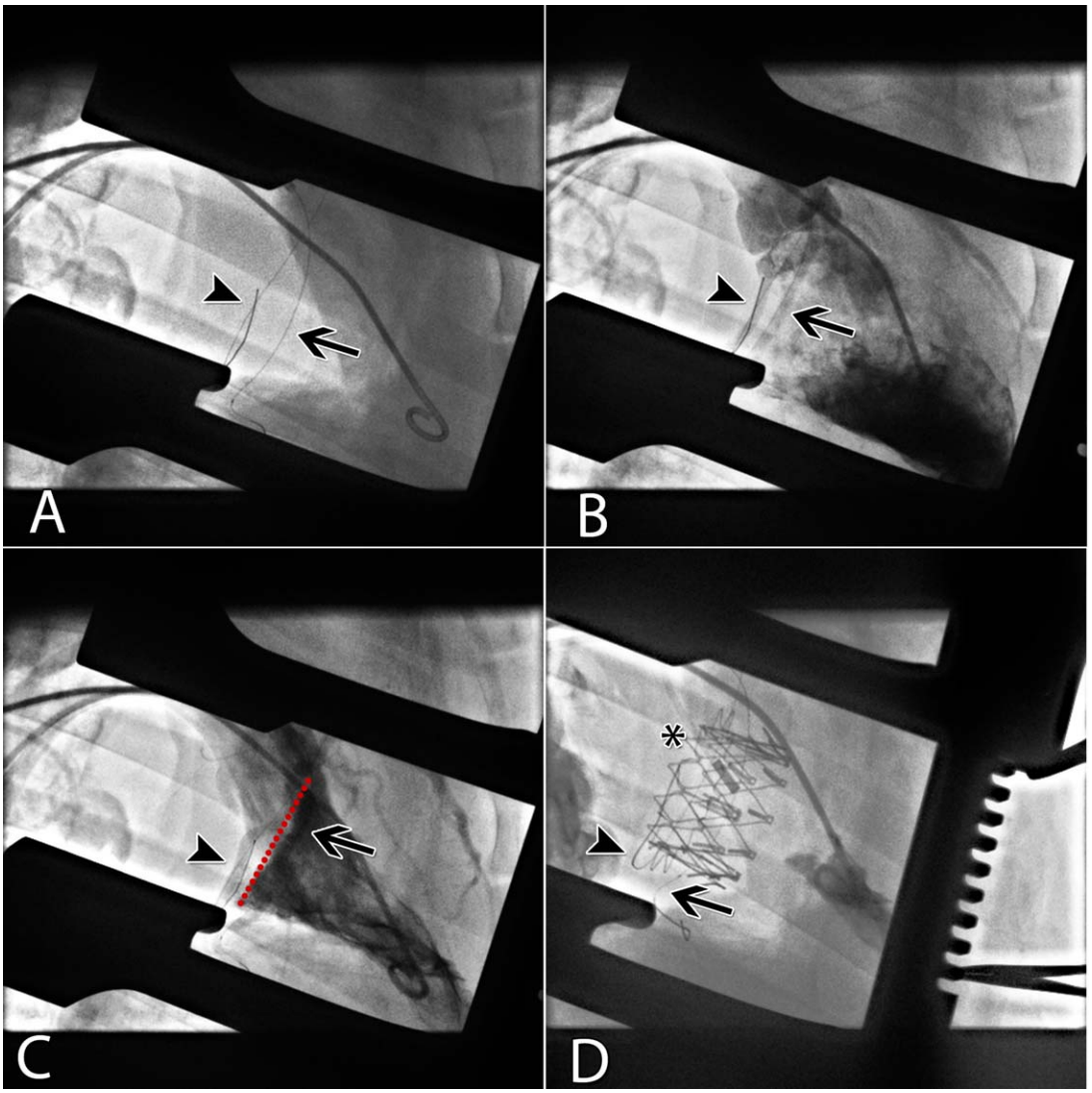

Fig. 11. Fluoroscopy images illustrating TMVI in an animal model using the novel concept of LCX-RCA plane. A: Guide-wires in LCX (arrow) and RCA (arrowhead). B: Left ventriculogram while guide-wires in place. C: LCX-RCA plane correlating with MAP (red dotted line) during left ventriculogram. D: Mitral Valve prosthesis (asterisk) implanted with the help of guide-wires in LCX and RCA. [Color figure can be viewed in the online issue, which is available at wileyonlinelibrary.com.]

the mitral valve annular plane. In the long term animal model reported by Benai et al., failure to position the valve occurred in 5 animals (14% of the cases), which is a significant percentage, and three out of seven animals had 2/4 PVL [3]. In another human case of TMVI, the implantation failed and caused severe PVL and the prosthesis had to be explanted and replaced with conventional surgery [6]. TEE remains crucial for intraprocedural guidance, but having a fluoroscopic confirmation of the mitral valve annular plane is highly desirable for optimum device delivery.

In this manuscript, we are proposing a novel concept. We suggest that the LCX-RCA plane has a constant correlation with the MAP, and that this correlation is preserved during the entire cardiac cycle. This could be applied during TMVI by first defining the LCX-RCA plane using either simultaneous contrast opacification or by insertion of radiopaque guide-wires in both coronaries; which can be easily done in the catheterization laboratory. Combined with preprocedural CT data defining the relationship between the LCX-RCA and MAP, the angiographic plane defined by the coronary arteries could then be used to ensure proper positioning of the mitral valve prosthesis before deployment. LAO 90° and RAO 30° projections were chosen for ergonomic convenience. Since most of the TMVI procedures reported

to-date were performed via transapical approach, positioning the C-arm in those projections is feasible from a practical standpoint. Based on the CT data acquired prior to the TMVI (including the separation and possibly the angle between both planes), it would be possible to define the anatomical position of the annulus with good precision in real-time and define the corresponding fluoroscopic angulation. Special software can be developed to serve that purpose, as has been the case for TAVR [26].

Figure 11 represents an animal model where the LCX-RCA plane was used to guide TMVI, by simultaneous insertion of radiopaque guide-wires in both coronaries. Of particular interest, the plane demarked by the valve prosthesis is in close relationship with the plane defined by the wires positioned in the LCX-RCA coronaries.

Limitations of this study include small sample size, which calls for larger studies in the future to confirm the reported findings. We also need further studies to analyze these relationships in patients with mitral valve pathologies. It is also not known whether the correlation between LCX-RCA and MAP would be affected by conduction abnormalities such as right or left bundle branch block and the difference in coronary position timing. This concern could also extend to the impact of pulmonary hypertension and the differences in right and left ventricular systolic function. Another important consideration is the historically proven saddle shaped configuration of the mitral valve, which makes a planar representation of its annulus quite challenging. However, recent studies have suggested that using a more planar D-shaped contour seems to be more convenient for the purpose of guiding transcatheter mitral valve procedures [27]. Finally, the usefulness of this novel technique will need to be tested to see if it improves device positioning and outcomes, as the observed geometric variability may exceed the acceptable positioning error for available valves.

In summary, we describe a novel method of identifying the MAP, which can be used in the cardiac catheterization laboratory to complement TEE in the context of TMVI procedural guidance.

REFERENCES

1. Fassa AA, Himbert D, Brochet E, Depoix JP, Cheong AP, Alkhoder S, Nataf P, Vahanian A. Transseptal transcatheter mitral valve implantation for severely calcified mitral stenosis. JACCCardiovascular Interv 2014;7:696–697.
2. Karimov JH, Massiello AL, Fukamachi K. Overview of current sutureless and transcatheter mitral valve replacement technology. Expert Rev Med Devices 2013;10:73–83.
3. Banai S, Verheye S, Cheung A, Schwartz M, Marko A, Lane R, Jolicoeur EM, Garceau P, Biner S, Tanguay JF, Edelman ER, White CJ. Transapical mitral implantation of the Tiara bioprosthesis: pre-clinical results. JACCCardiovascular Interv 2014;7:154–162.
4. Cheung A, Stub D, Moss R, Boone RH, Leipsic J, Verheye S, Banai S, Webb J. Transcatheter mitral valve implantation with Tiara bioprosthesis. EuroIntervention 2014;10 Suppl U:U115–U119.
5. Sinning JM, Mellert F, Schiller W, Welz A, Nickenig G, Hammerstingl C. Transcatheter mitral valve replacement using a balloon-expandable prosthesis in a patient with calcified native mitral valve stenosis. Eur Heart J 2013;34:2609.
6. Bruschi G, Botta L, Fratto P, Martinelli L. Failed valve-in-valve transcatheter mitral valve implantation. Eur J Cardiothorac Surg 2014;45:e127.
7. Backer O De, Piazza N, Banai S, Lutter G, Maisano F, Herrmann HC, Franzen OW, Sondergaard L. Percutaneous transcatheter mitral valve replacement: An overview of devices in preclinical and early clinical evaluation. Circ Interv 2014;7:400–409.
8. Bapat V, Buellesfeld L, Peterson MD, Hancock J, Reineke D, Buller C, Carrel T, Praz F, Rajani R, Fam N, Kim H, Redwood S, Young C, Munns C, Windecker S, Thomas M. Transcatheter mitral valve implantation (TMVI) using the Edwards FORTIS device. EuroIntervention 2014;10 Suppl U:U120–U128.
9. Lutter G, Lozonschi L, Ebner A, Gallo S, Marin y Kall C, Missov E Marchena E. de. First-in-human off-pump transcatheter mitral valve replacement. JACCCardiovascular Interv 2014;7:1077–1078.
10. Lozonschi L, Bombien R, Osaki S, Hu J, Snell D, Edwards NM, Cremer J, Lutter G. Transapical mitral valved stent implantation: a survival series in swine. J Thorac Cardiovasc Surg 2010;140:422–426.e1.
11. Piazza N, Bolling S, Moat N, Treede H. Medtronic transcatheter mitral valve replacement. EuroIntervention 2014;10 Suppl U:U112–U114.
12. Biasi AR de, Wong S-C, Salemi A. Reoperative 'valve-in-valve' transapical transcatheter mitral valve replacement in a high-risk patient with a recent transapical transcatheter aortic valve replacement and a degenerated bioprosthetic mitral valve. J Thorac Cardiovasc Surg 2014;148:e209–e210.
13. Kliger C, Angulo R, Maranan L, Kumar R, Jelnin V, Kronzon I, Fontana GP, Plestis K, Patel N, Perk G, Ruiz CE. Percutaneous complete repair of failed mitral valve prosthesis: Simultaneous closure of mitral paravalvular leaks and transcatheter mitral valve implantation - single-centre experience. EuroIntervention 2015;10:1336–1345.
14. Kaneko T, Swain JD, Loberman D, Welt FGP, Davidson MJ, Eisenhauer AC. Transjugular approach in valve-in-valve transcatheter mitral valve replacement: Direct route to the valve. Ann Thorac Surg 2014;97:e161–e163.
15. Kodali SK, Williams MR, Smith CR, Svensson LG, Webb JG, Makkar RR, Fontana GP, Dewey TM, Thourani VH, Pichard AD, Fischbein M, Szeto WY, Lim S, Greason KL, Teirstein PS, Malaisrie SC, Douglas PS, Hahn RT, Whisenant B, Zajarias A, Wang D, Akin JJ, Anderson WN, Leon MB. Two-Year Outcomes after Transcatheter or Surgical Aortic-Valve Replacement. N Engl J Med 2012;1686–1695.
16. Makkar RR, Fontana GP, Jilaihawi H, Kapadia S, Pichard AD, Douglas PS, Thourani VH, Babaliaros VC, Webb JG, Herrmann HC, Bavaria JE, Kodali S, Brown DL, Bowers B, Dewey TM, Svensson LG, Tuzcu M, Moses JW, Williams MR, Siegel RJ, Akin JJ, Anderson WN, Pocock S, Smith CR, Leon MB. Transcatheter aortic-valve replacement for inoperable severe aortic stenosis. N Engl J Med 2012;366:1696–1704.

17. Rodés-Cabau J, Webb JG, Cheung A, Ye J, Dumont E, Osten M, Feindel CM, Natarajan MK, Velianou JL, Martucci G, DeVarennes B, Chisholm R, Peterson M, Thompson CR, Wood D, Toggweiler S, Gurvitch R, Lichtenstein SV, Doyle D, DeLarochellière R, Teoh K, Chu V, Bainey K, Lachapelle K, Cheema A, Latter D, Dumesnil JG, Pibarot P, Horlick E. Long-term outcomes after transcatheter aortic valve implantation: Insights on prognostic factors and valve durability from the Canadian multicenter experience. J Am Coll Cardiol 2012;60: 1864–1875.
18. Kurra V, Kapadia SR, Tuzcu EM, Halliburton SS, Svensson L, Roselli EE, Schoenhagen P. Pre-procedural imaging of aortic root orientation and dimensions: Comparison between X-ray angiographic planar imaging and 3-dimensional multidetector row computed tomography. JACC Cardiovasc Interv 2010;3: 105–113. [Internet]. [cited 2014 Dec 15];:–. Available from: http://www.ncbi.nlm.nih.gov/pubmed/20129578
19. Litmanovich DE, Ghersin E, Burke DA, Popma J, Shahrzad M, Bankier AA. Imaging in Transcatheter Aortic Valve Replacement (TAVR): Role of the radiologist. Insights Imaging 2014;5: 123–145.
20. Nakamura K, Funabashi N, Naito S, Uehara M, Takaoka H, Kaseno K, Kumagai K, Oshima S, Kobayashi Y. Anatomical relationship of coronary sinus/great cardiac vein and left circumflex coronary artery along mitral annulus in atrial fibrillation before radiofrequency catheter ablation using 320-slice CT. Int J Cardiol 2013;168:5174–5181.
21. Spencer JH, Prahl G, Iaizzo PA. The prevalence of coronary sinus and left circumflex artery overlap in relation to the mitral valve. J Interv Cardiol 2014;27:308–316.
22. Choure AJ, Garcia MJ, Hesse B, Sevensma M, Maly G, Greenberg NL, Borzi L, Ellis S, Tuzcu EM, Kapadia SR. In vivo analysis of the anatomical relationship of coronary sinus to mitral annulus and left circumflex coronary artery using cardiac multidetector computed tomography: implications for percutaneous coronary sinus mitral annuloplasty. J Am Coll Cardiol 2006;48:1938–1945.
23. Gopal A, Shah A, Shareghi S, Bansal N, Nasir K, Gopal D, Budoff MJ, Shavelle DM. The role of cardiovascular computed tomographic angiography for coronary sinus mitral annuloplasty. J Invasive Cardiol 2010;22:67–73.
24. Bland JM, Altman DG. Statistical methods for assessing agreement between two methods of clinical measurement. Lancet 1986; 1:307–310.
25. Ghersin N, Abadi S, Sabbag A, Lamash Y, Anderson RH, Wolfson H, Lessick J. The three-dimensional geometric relationship between the mitral valvar annulus and the coronary arteries as seen from the perspective of the cardiac surgeon using cardiac computed tomography. Eur J Cardio-Thoracic Surg 2013; 44:1123–1130.
26. Lou J, Obuchowski NA, Krishnaswamy A, Popovic Z, Flamm SD, Kapadia SR, Svensson LG, Bolen MA, Desai MY, Halliburton SS, Tuzcu EM, Schoenhagen P. Manual, semiautomated, and fully automated measurement of the aortic annulus for planning of transcatheter aortic valve replacement (TAVR/TAVI): Analysis of interchangeability. J Cardiovasc Comput Tomogr 2015;9:42–49. [Internet]. [cited 2015 Jan 5]; Available from: http://www.ncbi.nlm.nih.gov/pubmed/25533222
27. Blanke P, Dvir D, Cheung A, Ye J, Levine RA, Precious B, Berger A, Stub D, Hague C, Murphy D, Thompson C, Munt B, Moss R, Boone R, Wood D, Pache G, Webb J, Leipsic J. A simplified D-shaped model of the mitral annulus to facilitate CT-based sizing before transcatheter mitral valve implantation. J Cardiovasc Comput Tomogr 2014;8:459–467.